JOURNAL OF GUIDANCE, CONTROL, AND DYNAMICS
Vol. 32, No. 1, January–February 2009

Event Triggers in Linear Covariance Analysis with Applications to Orbital Rendezvous

David K. Geller,* M. Ben Rose,† and David C. Woffinden†
Utah State University, Logan, Utah 84322

DOI: 10.2514/1.36834

The analytic expressions for a generic event trigger for a linear covariance analysis are developed. The event triggers are applied to the analysis of a common orbital rendezvous problem. Some unexpected results are observed and a flaw in an equation that is commonly used in standard linear covariance analysis applications is uncovered and remedied. A quantitative analysis of the effect of elevation-angle triggers for various rendezvous scenarios is presented.

Nomenclature

$\mathcal{C}_A$	=	covariance of augmented state vector
$\mathbf{F}^i_{\text{grav}}$	=	gravitational force in an inertial coordinate frame
$I_{n\times n}$	=	identity matrix
$\hat{P}$	=	flight computer covariance of navigation state error
$\mathbf{R}^{\text{lvlh}}$	=	position of chaser relative to an object centered rotating lvlh frame
$\mathbf{r}^i_o$	=	position of object in an inertial coordinate frame
$\mathbf{r}^i_c$	=	position of chaser in an inertial coordinate frame
$\mathcal{T}^a_b$	=	direction cosine matrix representing the orientation of the b frame with respect to the a frame
$\mathbf{V}^{\text{lvlh}}$	=	velocity of chaser relative to an object centered rotating lvlh frame
$\mathbf{v}^a$	=	vector represented in coordinate frame a
$\mathbf{v}^i_c$	=	velocity of chaser in an inertial coordinate frame
$\mathbf{v}^i_o$	=	velocity of object in an inertial coordinate frame
$\mathbf{x}$	=	true states
$\hat{\mathbf{x}}$	=	flight computer navigation states
$\bar{\mathbf{x}}$	=	reference states
$\tilde{\mathbf{z}}_k$	=	discrete noninertial measurements at time t_k
$\Delta\hat{\mathbf{u}}_j$	=	impulsive actuator commands issued by the flight computer at time t_j
$\Delta\mathbf{v}^i_{\text{com}}$	=	Δv command in an inertial coordinate frame
$\delta\mathbf{e}$	=	true navigation error
$\delta_{jj'}$	=	Kronecker delta function
$\delta(t-t')$	=	Dirac delta function
$\delta\mathbf{x}$	=	true state dispersions
$\delta\hat{\mathbf{x}}$	=	navigation state dispersions
$0_{m\times n}$	=	matrix of zeros
$\hat{}$	=	parameters, variables, and functions associated with the flight algorithms
$\tilde{}$	=	measured values
$\bar{}$	=	reference values
$[\boldsymbol{\epsilon}\times]$	=	cross product matrix defined by the ordinary cross product $[\epsilon\times]\mathbf{v} = \boldsymbol{\epsilon}\times\mathbf{v}$

I. Introduction

DISCRETE events, such as short impulsive maneuvers, sensor acquisition, and guidance, navigation, and control (GN&C) mode changes, can be triggered by onboard estimates of position, velocity, or orientation. The objective of this paper is to develop the analytic expressions that are needed to implement a generic event trigger in a linear covariance analysis.

An important application of an event trigger occurs in orbital rendezvous. Orbital rendezvous missions often have a coelliptic approach phase, where a chaser vehicle approaches an object from behind and below with a near constant altitude and relative velocity. A well-known orbital rendezvous technique is to trigger a terminal phase initiation (TPI) maneuver when the apparent elevation of the object reaches a predetermined value. When the object is at this elevation angle (as indicated by the onboard navigation), the TPI maneuver event is triggered and used to transfer the chaser to a position on the object v-bar (local horizontal). This technique was used in Gemini and Apollo, and is still used in shuttle missions [1–4].

There have recently been several relevant applications of linear covariance analysis to orbital rendezvous problems [5–8], but these applications have been limited because the effect of a TPI maneuver trigger could not be included in the analysis. This paper will show how the event triggers in a linear covariance analysis can be applied to TPI maneuvers for orbital rendezvous analysis.

A standard set of linear covariance analysis equations without event triggers is introduced in Sec. II and then applied to a generic orbital rendezvous problem in Sec. III. The expressions required to implement event triggers in a linear covariance analysis are developed in Sec. IV and applied to an orbital rendezvous problem in Sec. V. A detailed quantitative analysis of the effects of elevation-angle triggers for low-Earth-orbital rendezvous is given in Sec. VI.

II. Standard Linear Covariance Analysis

Figure 1 illustrates a generic GN&C Monte Carlo simulation. Before defining the variables in this figure, a brief summary is warranted. White noise processes $\mathbf{w}$, $\Delta\mathbf{w}_j$, $\boldsymbol{\nu}_k$, and discrete flight computer actuator commands $\Delta\hat{\mathbf{u}}_j$ drive truth models, which in turn generate the true state $\mathbf{x}$ of the system along with simulated sensor measurements $\tilde{\mathbf{z}}_k$. A navigation algorithm processes the sensor data and produces a navigation state $\hat{\mathbf{x}}$ and a navigation state error covariance $\hat{P}$. The navigation state is used by the targeting algorithm in the flight computer to generate discrete actuator commands. The key variables are the *true dispersions* from the reference $\delta\mathbf{x} = \mathbf{x} - \bar{\mathbf{x}}$, the *navigation dispersions* from the reference $\delta\hat{\mathbf{x}} = \hat{\mathbf{x}} - \bar{\mathbf{x}}$, and the *true navigation errors* $\delta\mathbf{e} = \delta\hat{\mathbf{x}} - \delta\mathbf{x}$. The covariance of the dispersions and navigation errors is often of primary interest.

A linear covariance analysis of the system in Fig. 1 is a technique that can produce the same statistical results as a Monte Carlo analysis but in a fraction of the time. A brief review of how to implement a linear covariance analysis of a generic GN&C system is given next. A more detailed description can be found in [6].

Received 25 January 2008; accepted for publication 15 July 2008.

*Assistant Professor, Mechanical and Aerospace Engineering. Senior Member AIAA.

†Graduate Student, Mechanical and Aerospace Engineering.

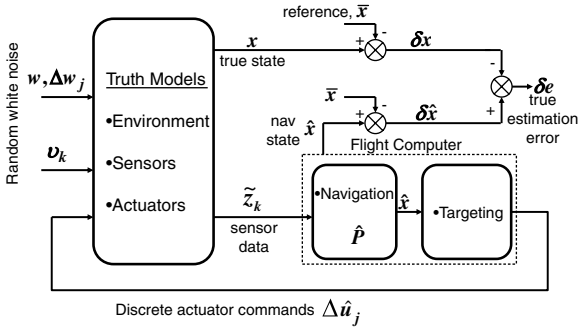

Fig. 1 Generic Monte Carlo simulation for GN&C analysis.

The linear covariance equations are based on a linearized version of the Monte Carlo simulation models. The dynamics of the Monte Carlo truth models shown in Fig. 1 are represented by

$$\dot{\mathbf{x}} = \mathbf{f}(\mathbf{x}, t) + \mathbf{w} \tag{1}$$

where $\mathbf{x}$ is a vector of n true states and $\mathbf{w}$ is a vector of zero-mean white noise processes with covariance $S_w(t)\delta(t - t')$. Sensors provide n_z discrete measurements $\tilde{\mathbf{z}}_k$ at times t_k where

$$\tilde{\mathbf{z}}_k = \mathbf{h}(\mathbf{x}_k, t_k) + \boldsymbol{\upsilon}_k \tag{2}$$

The covariance of the measurement noise is given by $R_\upsilon(t_k)\delta_{kk'}$. Instantaneous corrections to the state vector such as impulsive translation or rotational maneuvers are also allowed. Corrections at time t_j are represented as

$$\mathbf{x}_j^{+c} = \mathbf{x}_j^{-c} + \mathbf{d}(\mathbf{x}_j^{-c}, \Delta\hat{\mathbf{u}}_j, t_j) + \Delta\mathbf{w}_j \tag{3}$$

where the correction $\mathbf{d}(\mathbf{x}_j^{-c}, \Delta\hat{\mathbf{u}}_j, t_j)$ is a function of $\mathbf{x}_j^{-c}$, the true state just before the correction is applied, and $\Delta\hat{\mathbf{u}}_j$ is a vector of $n_{\Delta\hat{u}}$ instantaneous discrete corrective actuator commands issued by the flight computer. A random error $\Delta\mathbf{w}_j$ is also applied with the correction. The covariance of $\Delta\mathbf{w}_j$ is $S_{\Delta w}(t_j)\delta_{jj'}$.

The flight algorithms that produce the discrete actuator commands $\Delta\hat{\mathbf{u}}_j$ in Eq. (3) must also be defined. This includes both the navigation and targeting algorithms. The carets in these expressions refer to variables and functions related to flight algorithms, not just estimates or expected values.

The flight algorithms are divided into three sequential processes: 1) navigation state and state covariance propagation, 2) navigation state and state covariance update, and 3) navigation state and state covariance correction.

The navigation state and state covariance propagation algorithms are written as

$$\dot{\hat{\mathbf{x}}} = \hat{\mathbf{f}}(\hat{\mathbf{x}}, t) \tag{4}$$

$$\dot{\hat{P}} = \hat{F}_{\hat{x}}\hat{P} + \hat{P}\hat{F}_{\hat{x}}^T + \hat{S}_w \tag{5}$$

where $\hat{\mathbf{x}}$ is the navigation state of dimension n. $\hat{P}$ represents the flight computer's assessment of the navigation state error covariance matrix, and $\hat{F}_{\hat{x}}$ are the partial derivatives of $\hat{\mathbf{f}}$ with respect to $\hat{\mathbf{x}}$. Unmodeled dynamics are represented by $\hat{S}_w$.

The navigation state and state covariance update algorithms [9] can be written as

$$\hat{\mathbf{x}}_k^+ = \hat{\mathbf{x}}_k^- + \hat{K}(t_k)[\tilde{\mathbf{z}}_k - \hat{\mathbf{h}}(\hat{\mathbf{x}}_k, t_k)] \tag{6}$$

$$\hat{P}(t_k^+) = [I - \hat{K}(t_k)\hat{H}_{\hat{x}}(t_k)]\hat{P}(t_k^-)[I - \hat{K}(t_k)\hat{H}_{\hat{x}}(t_k)]^T + \hat{K}(t_k)\hat{R}_\upsilon(t_k)\hat{K}^T(t_k) \tag{7}$$

where the Joseph formulation [10] is used for the covariance update and the Kalman gain $\hat{K}(t_k)$ is given by

$$\hat{K}(t_k) = \hat{P}(t_k)\hat{H}_{\hat{x}}^T(t_k)[\hat{H}_{\hat{x}}(t_k)\hat{P}(t_k)\hat{H}_{\hat{x}}^T(t_k) + \hat{R}_\upsilon(t_k)]^{-1} \tag{8}$$

The measurement sensitivity matrix is given by $\hat{H}_{\hat{x}}$ and the measurement noise covariance is $\hat{R}_\upsilon$.

When an instantaneous state correction as in Eq. (3) occurs, the navigation state must also be corrected. The correction algorithm can be written as

$$\hat{\mathbf{x}}_j^{+c} = \hat{\mathbf{x}}_j^{-c} + \hat{\mathbf{d}}(\hat{\mathbf{x}}^{-c}, \Delta\hat{\mathbf{u}}_j, t_j) \tag{9}$$

$$\hat{P}(t_j^{+c}) = [I + \hat{D}_{\hat{x}}(t_j)]\hat{P}^{-c}(t_j)[I + \hat{D}_{\hat{x}}(t_j)]^T + \hat{S}_{\Delta w}(t_j) \tag{10}$$

where $\hat{D}_{\hat{x}}$ are the partial derivatives of $\hat{\mathbf{d}}$ with respect to $\hat{\mathbf{x}}$. For each, an instantaneous correction $\hat{S}_{\Delta w}$ corresponds to the noise component of the $\Delta\hat{\mathbf{u}}_j$ application error.

The targeting algorithms use the most recent value of the navigation state to compute discrete actuator commands

$$\Delta\hat{\mathbf{u}}_j = \Delta\hat{\mathbf{g}}(\hat{\mathbf{x}}_j^{-c}, t_j) \tag{11}$$

where $\Delta\hat{\mathbf{g}}(\hat{\mathbf{x}}_j^{-c}, t_j)$ represents the algorithm for discrete instantaneous commanding.

For a linear covariance analysis, the preceding equations are linearized about a reference trajectory defined by $\bar{\mathbf{x}}(t)$ to produce a set of equations that describe the time-evolution of the true state dispersions from the reference $\delta\mathbf{x}(t) = \mathbf{x}(t) - \bar{\mathbf{x}}(t)$ and the time evolution of the navigation state dispersions from the reference $\delta\hat{\mathbf{x}}(t) = \hat{\mathbf{x}}(t) - \bar{\mathbf{x}}(t)$, as shown in Fig. 1.

The propagation equations, Eqs. (1) and (4), are linearized to produce

$$\delta\dot{\mathbf{x}} = F_x\delta\mathbf{x} + \mathbf{w} \tag{12}$$

$$\delta\dot{\hat{\mathbf{x}}} = \hat{F}_{\hat{x}}\delta\hat{\mathbf{x}} \tag{13}$$

where the partial derivatives are evaluated along the reference trajectory.

The state update given by Eq. (6) and the measurement equation in Eq. (2) are also linearized about the reference trajectory to produce

$$\delta\mathbf{x}_k^+ = \delta\mathbf{x}_k^- \tag{14}$$

$$\delta\hat{\mathbf{x}}_k^+ = \hat{K}(t_k)H_x(t_k)\delta\mathbf{x}_k^- + [I - \hat{K}(t_k)\hat{H}_{\hat{x}}(t_k)]\delta\hat{\mathbf{x}}_k^- + \hat{K}(t_k)\boldsymbol{\upsilon}_k \tag{15}$$

where the dispersions $\delta\mathbf{x}$ are unaffected by measurement updates.

Finally, the state corrections in Eqs. (3) and (9) are linearized to produce

$$\delta\mathbf{x}_j^{+c} = [I + D_x(t_j)]\delta\mathbf{x}_j^{-c} + D_{\Delta\hat{u}}(t_j)\Delta\hat{G}_{\hat{x}}(t_j)\delta\hat{\mathbf{x}}_j^{-c} + \Delta\mathbf{w}_j \tag{16}$$

$$\delta\hat{\mathbf{x}}_j^{+c} = [I + \hat{D}_{\hat{x}}(t_j) + \hat{D}_{\Delta\hat{u}}(t_j)\Delta\hat{G}_{\hat{x}}(t_j)]\delta\hat{\mathbf{x}}_j^{-c} \tag{17}$$

where, again, the partial derivatives are evaluated along the reference trajectory.

Next, we define an augmented state vector [10] $\mathbf{X}$ consisting of the true state dispersions and navigation state dispersions.

$$\mathbf{X} = \begin{bmatrix} \delta\mathbf{x} \\ \delta\hat{\mathbf{x}} \end{bmatrix} \tag{18}$$

Equations (12–17) may now be written in the following compact form:

$$\dot{\mathbf{X}} = \mathcal{F}\mathbf{X} + \mathcal{W}\mathbf{w} \tag{19}$$

$$\mathbf{X}_k^+ = \mathcal{A}_k\mathbf{X}_k^- + \mathcal{B}_k\boldsymbol{\upsilon}_k \tag{20}$$

$$\mathbf{X}_j^{+c} = \mathcal{D}_j\mathbf{X}_j^{-c} + \mathcal{N}_j\Delta\mathbf{w}_j \tag{21}$$

where

$$\mathcal{F} = \begin{pmatrix} F_x & 0_{n\times n} \\ 0_{n\times n} & \hat{F}_{\hat{x}} \end{pmatrix}, \qquad \mathcal{W} = \begin{pmatrix} I_{n\times n} \\ 0_{n\times n} \end{pmatrix} \tag{22}$$

$$\mathcal{A}_k = \begin{pmatrix} I_{n\times n} & 0_{n\times n} \\ \hat{K}(t_k)H_x(t_k) & I_{n\times n} - \hat{K}(t_k)\hat{H}_{\hat{x}} \end{pmatrix}, \qquad \mathcal{B}_k = \begin{pmatrix} 0_{n\times n_z} \\ \hat{K}(t_k) \end{pmatrix} \tag{23}$$

$$\mathcal{D}_j = \begin{pmatrix} I_{n\times n} + D_x(t_j) & D_{\Delta\hat{u}}(t_j)\Delta\hat{G}_{\hat{x}}(t_j) \\ 0_{n\times n} & I_{\hat{n}\times\hat{n}} + \hat{D}_{\hat{x}}(t_j) + \hat{D}_{\Delta\hat{u}}(t_j)\Delta\hat{G}_{\hat{x}}(t_j) \end{pmatrix} \tag{24}$$

$$\mathcal{N}_j = \begin{pmatrix} I_{n\times n} \\ 0_{\hat{n}\times n} \end{pmatrix} \tag{25}$$

We can now formulate the covariance equations for the entire linear covariance analysis. Remember that, with respect to the Monte Carlo simulation, the true state $\mathbf{x}(t)$ and the navigated state $\hat{\mathbf{x}}(t)$ are random processes that vary from one Monte Carlo sample to the next. Since $E[\mathbf{x}(t)] = E[\bar{\mathbf{x}}(t)]$ and $E[\hat{\mathbf{x}}(t)] = E[\mathbf{x}(t)]$, the true and navigation state dispersions $\delta\mathbf{x}(t)$ and $\delta\hat{\mathbf{x}}(t)$ will have zero means, and thus $E[\mathbf{X}(t)] = \mathbf{0}$. The covariance of the augmented state $\mathbf{X}(t)$, $\mathcal{C}_A = E[\mathbf{X}(t)\mathbf{X}^T(t)]$, can be obtained with the following set of covariance propagation, update, and correction equations:

$$\dot{\mathcal{C}}_A = \mathcal{F}\mathcal{C}_A + \mathcal{C}_A\mathcal{F}^T + \mathcal{W}S_w\mathcal{W}^T \tag{26}$$

$$\mathcal{C}_A(t_k^+) = \mathcal{A}_k\mathcal{C}_A(t_k^-)\mathcal{A}_k^T + \mathcal{B}_kR_v(t_k)\mathcal{B}_k^T \tag{27}$$

$$\mathcal{C}_A(t_j^{+c}) = \mathcal{D}_j\mathcal{C}_A(t_j^{-c})\mathcal{D}_j^T + \mathcal{N}_jS_{\Delta w}(t_j)\mathcal{N}_j^T \tag{28}$$

where it is assumed that $\mathbf{w}$, $\Delta\mathbf{w}_j$, and $\boldsymbol{\nu}_k$ are mutually uncorrelated.

When the onboard flight computer covariance equations, Eqs. (5), (7), (8), and (10), are appended to Eqs. (26–28), a complete set of linear covariance analysis equations is formed.

III. Orbital Rendezvous Application

Orbital rendezvous missions often have a coelliptic approach phase where the chaser approaches an object from behind and below with a near constant altitude and relative velocity. At the proper time, a terminal phase initiation maneuver is executed and used to transfer the chaser to a position on the object v-bar.

To simulate this rendezvous scenario, a relatively simple orbital rendezvous model is developed. The true state vector consists of the inertial positions and velocities of the chaser vehicle and a resident space object:

$$\mathbf{x} = \begin{pmatrix} \mathbf{r}_o^i \\ \mathbf{v}_o^i \\ \mathbf{r}_c^i \\ \mathbf{v}_c^i \end{pmatrix} \tag{29}$$

The associated model of the true dynamics is given by

$$\dot{\mathbf{x}} = \begin{pmatrix} \dot{\mathbf{r}}_o^i \\ \dot{\mathbf{v}}_o^i \\ \dot{\mathbf{r}}_c^i \\ \dot{\mathbf{v}}_c^i \end{pmatrix} = \begin{pmatrix} \mathbf{v}_o^i \\ \mathbf{F}_{\text{grav}_o}^i(\mathbf{r}_o^i)/m_o + \mathbf{w}_{g_o} \\ \mathbf{v}_c^i \\ \mathbf{F}_{\text{grav}_c}^i(\mathbf{r}_c^i)/m_c + \mathbf{w}_{g_c} \end{pmatrix} \tag{30}$$

where m_o is the resident space object mass and m_c is the chaser mass. Random disturbances $\mathbf{w}_{g_o}$ and $\mathbf{w}_{g_c}$ represent higher-order unmodeled accelerations. The covariances of the disturbances are $S_{g_o}\delta(t-t')$ and $S_{g_c}\delta(t-t')$, respectively.

A simple Lidar model is used for relative position measurements

$$\tilde{\mathbf{z}} = \mathbf{r}_o^i - \mathbf{r}_c^i + \boldsymbol{\nu}_{\text{lidar}} \tag{31}$$

where the covariance of the Lidar measurement noise is $R_{\boldsymbol{\nu}_{\text{lidar}}}$.

The navigation state propagation equations are given by

$$\dot{\hat{\mathbf{r}}}_o^i = \hat{\mathbf{v}}_o^i \tag{32}$$

$$\dot{\hat{\mathbf{v}}}_o^i = \hat{\mathbf{F}}_{\text{grav}_o}^i(\hat{\mathbf{r}}_o^i)/\hat{m}_o \tag{33}$$

$$\dot{\hat{\mathbf{r}}}_c^i = \hat{\mathbf{v}}_c^i \tag{34}$$

$$\dot{\hat{\mathbf{v}}}_c^i = \hat{\mathbf{F}}_{\text{grav}_c}^i(\hat{\mathbf{r}}_c^i)/\hat{m}_c \tag{35}$$

and the navigation state covariance propagation equation is

$$\dot{\hat{P}} = \hat{F}_{\hat{x}}\hat{P} + \hat{P}\hat{F}_{\hat{x}}^T + \hat{S}_w \tag{36}$$

where the partial derivatives $\hat{F}_{\hat{x}}$ and the state process noise covariance $\hat{S}_w$ are given in the Appendix. The navigation state covariance update equation is given by

$$\hat{P}(t_k^+) = [I - \hat{K}(t_k)\hat{H}_{\hat{x}}(t_k)]\hat{P}(t_k^-)[I - \hat{K}(t_k)\hat{H}_{\hat{x}}(t_k)]^T + \hat{K}(t_k)\hat{R}_v(t_k)\hat{K}^T(t_k) \tag{37}$$

where the Kalman gain $\hat{K}(t_k)$ is given in Eq. (8), and the measurement sensitivity matrice $\hat{H}_{\hat{x}}$ is

$$\hat{H}_{\hat{x}} = \begin{pmatrix} I_{n\times n} & 0_{n\times n} & -I_{n\times n} & 0_{n\times n} \end{pmatrix} \tag{38}$$

Discrete impulsive Δ-v maneuvers are modeled as

$$(\mathbf{v}_c^i)^{+c} = (\mathbf{v}_c^i)^{-c} + \Delta\hat{\mathbf{v}}_{\text{com}}^i + \Delta\mathbf{w}_{\Delta v} \tag{39}$$

where the actuator command $\Delta\hat{\mathbf{v}}_{\text{com}}^i$ generated by the flight computer is given in Eq. (46), and the covariance of the actuation noise is given by $S_{\Delta w_{\Delta v}}$. When a correction is made to the navigation state, the navigation state covariance matrix is also corrected

$$\hat{P}(t_j^{+c}) = [I + \hat{D}_{\hat{x}}(t_j)]\hat{P}(t_j^{-c})[I + \hat{D}_{\hat{x}}(t_j)]^T + \hat{S}_{\Delta w}(t_j) \tag{40}$$

where the partial derivative $\hat{D}_{\hat{x}}$ and the covariance matrix $\hat{S}_{\Delta w}$ are given in the Appendix.

A simple maneuver-targeting algorithm based on the Clohessy–Wiltshire (CW) equations [11] is used to compute $\Delta\hat{\mathbf{v}}_{\text{com}}^i$. (A more sophisticated algorithm such as Lambert targeting can be easily incorporated if needed.) In a local-vertical/local-horizontal (lvlh) coordinate frame, the CW equations can be written as

$$\begin{pmatrix} \hat{\mathbf{R}}^{\text{lvlh}}(t_f) \\ \hat{\mathbf{V}}^{\text{lvlh}}(t_f) \end{pmatrix} = \begin{pmatrix} \Phi_{rr} & \Phi_{rv} \\ \Phi_{vr} & \Phi_{vv} \end{pmatrix} \begin{pmatrix} \hat{\mathbf{R}}^{\text{lvlh}}(t_0) \\ \hat{\mathbf{V}}^{\text{lvlh}}(t_0) \end{pmatrix} \tag{41}$$

where

$$\hat{\mathbf{R}}^{\text{lvlh}}(t_0) = \hat{\mathcal{T}}_{\text{lvlh}}^i(\hat{\mathbf{r}}_c^i - \hat{\mathbf{r}}_o^i) \tag{42}$$

$$\hat{\mathbf{V}}^{\text{lvlh}}(t_0) = \hat{\mathcal{T}}_{\text{lvlh}}^i[\hat{\mathbf{v}}_c^i - \hat{\mathbf{v}}_o^i - \hat{\boldsymbol{\omega}}_{\text{orb}}^i \times (\hat{\mathbf{r}}_c^i - \hat{\mathbf{r}}_o^i)] \tag{43}$$

$$\hat{\boldsymbol{\omega}}_{\text{orb}}^i = \hat{\mathbf{v}}_o^i \times \hat{\mathbf{r}}_o^i / \|\hat{\mathbf{r}}_o^i\|^2 \tag{44}$$

To achieve a desired relative position $\hat{\mathbf{R}}_{\text{des}}^{\text{lvlh}}$ at time t_f, the required $\Delta\mathbf{v}$ at time t_0 is

$$\Delta\hat{\mathbf{v}}_{\text{req}}^{\text{lvlh}} = \Phi_{rv}^{-1}[\hat{\mathbf{R}}_{\text{des}}^{\text{lvlh}} - \Phi_{rr}\hat{\mathcal{T}}_{\text{lvlh}}^i(\hat{\mathbf{r}}_c^i - \hat{\mathbf{r}}_o^i)] - \hat{\mathcal{T}}_{\text{lvlh}}^i[\hat{\mathbf{v}}_c^i - \hat{\mathbf{v}}_o^i - \hat{\boldsymbol{\omega}}_{\text{orb}}^i \times (\hat{\mathbf{r}}_c^i - \hat{\mathbf{r}}_o^i)] \tag{45}$$

The $\Delta\mathbf{v}$ command that goes out to the actuators is the required $\Delta\mathbf{v}$ transformed to inertial frame:

$$\Delta\hat{\mathbf{v}}^i_{\text{com}} = \hat{\mathcal{T}}^{\text{lvlh}}_i \Delta\hat{\mathbf{v}}^{\text{lvlh}}_{\text{req}} \tag{46}$$

To conduct a linear covariance of this orbital rendezvous scenario, the preceding models are used to populate the matrices in the linear covariance equations given in Eqs. (26–28). As the augmented state covariance matrix $\mathcal{C}_A$ is propagated, updated, and corrected, the covariance of the relative position dispersions in lvlh coordinates can be computed using

$$D^{\text{lvlh}} = H_{\text{lvlh}} \mathcal{C}_A H^T_{\text{lvlh}} \tag{47}$$

where

$$H_{\text{lvlh}} = (\,\mathcal{T}^i_{\text{lvlh}}(\bar{\mathbf{r}}^i_o, \bar{\mathbf{v}}^i_o) \quad 0_{3\times3} \quad -\mathcal{T}^i_{\text{lvlh}}(\bar{\mathbf{r}}^i_o, \bar{\mathbf{v}}^i_o) \quad 0_{3\times3} \quad 0_{3\times n}\,) \tag{48}$$

For near-circular orbits, the inertial-to-lvlh transformation $\mathcal{T}^i_{\text{lvlh}}(\bar{\mathbf{r}}^i_o, \bar{\mathbf{v}}^i_o)$ is given by

$$\mathcal{T}^{\,i}_{\text{lvlh}}(\bar{\mathbf{r}}^i_o, \bar{\mathbf{v}}^i_o) = (\,\mathbf{i}^i_{\mathbf{v}_\mathbf{o}} \quad \mathbf{i}^i_{\mathbf{h}_\mathbf{o}} \quad \mathbf{i}^i_{\mathbf{r}_\mathbf{o}}\,)^T \tag{49}$$

where $\mathbf{i}^i_{\mathbf{v}_\mathbf{o}} = \mathbf{v}^\mathbf{i}_\mathbf{o}/|\mathbf{v}^\mathbf{i}_\mathbf{o}|$, $\mathbf{i}^i_{\mathbf{h}_\mathbf{o}} = \mathbf{r}^\mathbf{i}_\mathbf{o} \times \mathbf{v}^\mathbf{i}_\mathbf{o}/|\mathbf{r}^\mathbf{i}_\mathbf{o} \times \mathbf{v}^\mathbf{i}_\mathbf{o}|$, and $\mathbf{i}^i_{\mathbf{r}_\mathbf{o}} = \mathbf{r}^\mathbf{i}_\mathbf{o}/|\mathbf{r}^\mathbf{i}_\mathbf{o}|$. A more complicated expression for $\mathcal{T}^i_{\text{lvlh}}(\bar{\mathbf{r}}^i_o, \bar{\mathbf{v}}^i_o)$ can be easily developed for orbits with arbitrary eccentricity.

Figure 2 illustrates what we might expect for this type of orbital rendezvous problem. The figure shows a nominal trajectory with two Monte Carlo samples. In all cases, the TPI maneuvers transfer the chaser to the desired position to within a few meters of the resident space object. Figure 2 also shows the anticipated covariance ellipses.

When we employ linear covariance analysis, the covariance ellipses are very similar to what is expected. This is illustrated in Fig. 3. The linear covariance analysis results clearly show that the relative position dispersions are driven to small values at the desired position.

In this particular orbital rendezvous scenario, it was assumed that the TPI maneuver occurred at a preselected fixed time. However, in many rendezvous missions, the TPI maneuver is triggered on an elevation-angle condition [1–4]. Implementing an elevation-angle trigger in a Monte Carlo analysis is a simple matter, but implementing an event trigger in a linear covariance analysis presents a challenge.

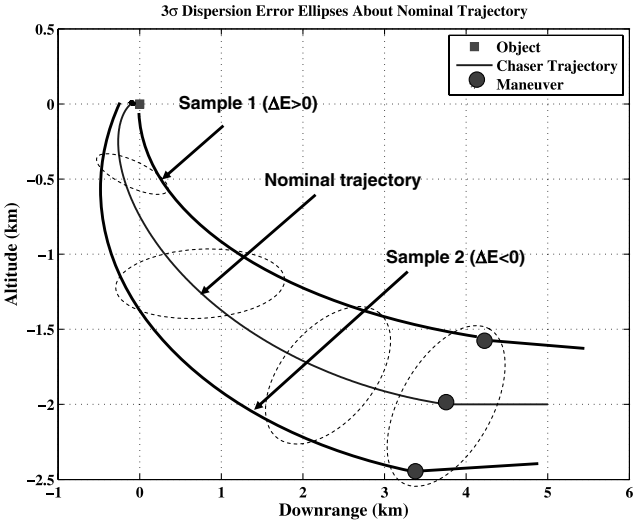

Fig. 2 Example of two Monte Carlo samples of a 2 km coelliptic approach. TPI occurs at a fixed maneuver time and initiates a 130 deg orbital (inertial) transfer. Navigation errors are <3 m 3-σ, and Δv execution errors are <3 mm/s 3-σ. Sample 1 has a slightly higher orbital energy than the nominal and therefore initiates the transfer further downrange. The opposite is true for sample 2. Anticipated dispersion covariance ellipses are also shown.

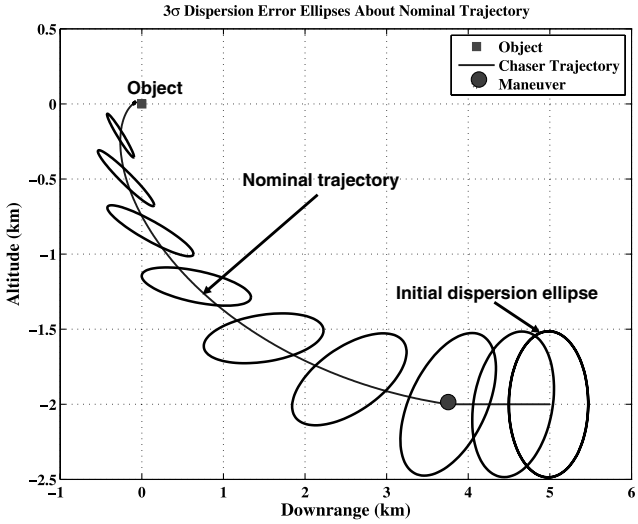

Fig. 3 Linear covariance analysis results for a 2 km coelliptic approach. TPI occurs at a fixed maneuver time and initiates a 130 deg orbital (inertial) transfer. Navigation errors are <3 m 3-σ, and Δv execution errors are <3 mm/s 3-σ.

IV. Event Triggers

An event trigger is a condition or constraint represented as a function of the estimated state

$$\Psi[\hat{\mathbf{x}}(t_e)] = 0 \tag{50}$$

When the condition or constraint is satisfied, it triggers a specific discrete event that occurs at time t_e. Examples of GN&C events include discrete maneuvers, sensor changes, and general GN&C mode changes. Examples of triggers include estimates of spacecraft altitude, speed, downrange position, or the apparent elevation angle of a second spacecraft. To determine how to implement an event trigger in a linear covariance analysis, it is useful to first look at the problem from the perspective of a Monte Carlo analysis.

In a Monte Carlo analysis, the time t_e at which the event occurs and the associated state estimate $\hat{\mathbf{x}}(t_e)$ for a given sample must satisfy Eq. (50). At the nominal time $\bar{t}_e$ of the event, the true and estimated states for a given sample are given by

$$\mathbf{x}\,(t_e) = \bar{\mathbf{x}}(\bar{t}_e) + \delta\mathbf{x}(\bar{t}_e) \tag{51}$$

$$\hat{\mathbf{x}}(\bar{t}_e) = \bar{\mathbf{x}}(\bar{t}_e) + \delta\hat{\mathbf{x}}(\bar{t}_e) \tag{52}$$

The trigger condition is generally not met at the nominal time,

$$\Psi[\hat{\mathbf{x}}(\bar{t}_e)] \neq 0 \tag{53}$$

However, at some time after (or before) the nominal time of the event, the estimated state will satisfy the trigger in Eq. (50), and if the difference between the event time and the nominal event time is small, the estimated and true states at time t_e can be written as

$$\mathbf{x}\,(t_e) = \mathbf{x}(\bar{t}_e) + \dot{\mathbf{x}}(\bar{t}_e)[t_e - \bar{t}_e] \tag{54}$$

$$\hat{\mathbf{x}}(t_e) = \hat{\mathbf{x}}(\bar{t}_e) + \dot{\hat{\mathbf{x}}}(\bar{t}_e)[t_e - \bar{t}_e] \tag{55}$$

where

$$\dot{\mathbf{x}}(\bar{t}_e) \approx \dot{\bar{\mathbf{x}}}(\bar{t}_e) + \delta\dot{\mathbf{x}}(\bar{t}_e) \tag{56}$$

$$\dot{\hat{\mathbf{x}}}(\bar{t}_e) \approx \dot{\bar{\mathbf{x}}}(\bar{t}_e) + \delta\dot{\hat{\mathbf{x}}}(\bar{t}_e) \tag{57}$$

Substituting Eqs. (52) and (57) into Eq. (55), and Eqs. (51) and (56) into Eq. (54), and neglecting second-order terms produces

$$\mathbf{x}(t_e) = \bar{\mathbf{x}}(\bar{t}_e) + \delta\mathbf{x}(\bar{t}_e) + \dot{\bar{\mathbf{x}}}(\bar{t}_e)\delta t_e \tag{58}$$

$$\hat{\mathbf{x}}(t_e) = \bar{\mathbf{x}}(\bar{t}_e) + \delta\hat{\mathbf{x}}(\bar{t}_e) + \dot{\bar{\mathbf{x}}}(\bar{t}_e)\delta t_e \tag{59}$$

where $\delta t_e = t_e - \bar{t}_e$.

Substituting Eq. (59) into Eq. (50) and expanding to first order produces

$$0 = \Psi[\bar{\mathbf{x}}(\bar{t}_e)] + \Psi_x[\delta\hat{\mathbf{x}}(\bar{t}_e) + \dot{\bar{\mathbf{x}}}(\bar{t}_e)\delta t_e] \tag{60}$$

where

$$\Psi_x = \left.\frac{\partial\Psi}{\partial x}\right|_{\bar{\mathbf{x}}}$$

Noting that $\Psi[\bar{\mathbf{x}}(\bar{t}_e)] = 0$, we can solve Eq. (60) for δt_e

$$\delta t_e = -[\Psi_x\dot{\bar{\mathbf{x}}}(\bar{t}_e)]^{-1}\Psi_x\delta\hat{\mathbf{x}}(\bar{t}_e) = M\delta\hat{\mathbf{x}}(\bar{t}_e) \tag{61}$$

Equation (61) is an important expression because it represents to first order the difference between the time the event occurs for the nominal trajectory and the time the event occurs for a Monte Carlo sample.

If we write the event time variation as a function of the augmented state $\mathbf{X}(\bar{t}_e)$

$$\delta t_e = 0_{1\times n}\delta\mathbf{x}(\bar{t}_e) + M\delta\hat{\mathbf{x}}(\bar{t}_e) = (\,0_{1\times n} \quad M\,)\mathbf{X}(\bar{t}_e) \tag{62}$$

the variance of the event time can be determined by squaring Eq. (62) and taking the expected value over all Monte Carlo samples at time $\bar{t}_e$:

$$\sigma^2_{\bar{t}_e} = (\,0_{1\times n} \quad M\,)\mathcal{C}_A(\bar{t}_e)(\,0_{1\times n} \quad M\,)^T \tag{63}$$

where $\mathcal{C}_A(\bar{t}_e)$ is the covariance of the augmented state time $t_{\bar{e}}$

$$\mathcal{C}_A(\bar{t}_e) = E[\mathbf{X}(\bar{t}_e)\mathbf{X}^T(\bar{t}_e)] \tag{64}$$

Equation (63) is another important expression because it represents the variance of the event time as a function of the state covariance at the nominal event time and the nominal trajectory.

From a Monte Carlo perspective, the next step is to collect all the estimated and true states at their respective event trigger times and evaluate the covariance of these states. Analytically, this is achieved by first substituting the event time variation in Eq. (61) back into Eqs. (58) and (59) to obtain the states at their respective event trigger times:

$$\mathbf{x}(t_e) = \bar{\mathbf{x}}(\bar{t}_e) + \delta\mathbf{x}(\bar{t}_e) + \dot{\bar{\mathbf{x}}}(\bar{t}_e)M\delta\hat{\mathbf{x}}(\bar{t}_e) \tag{65}$$

$$\hat{\mathbf{x}}(t_e) = \bar{\mathbf{x}}(\bar{t}_e) + \delta\hat{\mathbf{x}}(\bar{t}_e) + \dot{\bar{\mathbf{x}}}(\bar{t}_e)M\delta\hat{\mathbf{x}}(\bar{t}_e) \tag{66}$$

Because the mean values of the navigation dispersions $\delta\hat{\mathbf{x}}(\bar{t}_e)$ and true dispersions $\delta\mathbf{x}(\bar{t}_e)$ are zero at the nominal event time, the mean values of the states at the event trigger times are equal to the nominal states at the nominal event time:

$$E[\hat{\mathbf{x}}(t_e)] = E[\mathbf{x}(t_e)] = \bar{\mathbf{x}}(\bar{t}_e)$$

This is important because it allows us to analytically compute the covariance of the states at the trigger times. First, let the augmented state at the trigger time be defined as

$$\mathbf{X}(t_e) = \begin{pmatrix}\delta\mathbf{x}(t_e)\\ \delta\hat{\mathbf{x}}(t_e)\end{pmatrix} = \begin{pmatrix}\mathbf{x}(t_e) - \bar{\mathbf{x}}(\bar{t}_e)\\ \hat{\mathbf{x}}(t_e) - \bar{\mathbf{x}}(\bar{t}_e)\end{pmatrix} = \begin{pmatrix}\delta\mathbf{x}(\bar{t}_e) + \dot{\bar{\mathbf{x}}}(\bar{t}_e)M\delta\hat{\mathbf{x}}(\bar{t}_e)\\ \delta\hat{\mathbf{x}}(\bar{t}_e) + \dot{\bar{\mathbf{x}}}(\bar{t}_e)M\delta\hat{\mathbf{x}}(\bar{t}_e)\end{pmatrix} \tag{67}$$

or

$$\mathbf{X}(t_e) = \begin{pmatrix} I_{n\times n} & \dot{\bar{\mathbf{x}}}(\bar{t}_e)M \\ 0_{n\times n} & I_{n\times n} + \dot{\bar{\mathbf{x}}}(\bar{t}_e)M\end{pmatrix}\mathbf{X}(\bar{t}_e) \tag{68}$$

Because the mean value of $\mathbf{X}(t_e)$ is zero, the covariance of the augmented states immediately after the event trigger times is

$$\mathcal{C}^+_A(\bar{t}_e) = E[\mathbf{X}(t_e)\mathbf{X}^T(t_e)] = \Phi_S\mathcal{C}_A(\bar{t}_e)\Phi^T_S \tag{69}$$

where the covariance shaping matrix Φ_S is given by

$$\Phi_S = \begin{pmatrix} I_{n\times n} & \dot{\bar{\mathbf{x}}}(\bar{t}_e)M \\ 0_{n\times n} & I_{n\times n} + \dot{\bar{\mathbf{x}}}(\bar{t}_e)M\end{pmatrix} \tag{70}$$

The term in the lower right corner of the shaping matrix, $[I_{n\times n} + \dot{\bar{\mathbf{x}}}(\bar{t}_e)M]$, is sometimes called the projection matrix.

It is important to notice that $\mathcal{C}^+_A(\bar{t}_e)$ is the covariance of an ensemble of states with different event trigger times, and so it may at first appear difficult to assign one single time to the covariance $\mathcal{C}^+_A(\bar{t}_e)$. However, from a Monte Carlo analysis perspective, we can imagine resetting the simulation clock to a common time $\bar{t}_e$ for each sample as it triggers an event. All subsequent results are then measured with respect to the common time $\bar{t}_e$, and the state covariance at $\bar{t}_e$ is given by Eq. (69).

Notice also that because the true navigation error is defined as

$$\delta\mathbf{e} = \delta\mathbf{x} - \delta\hat{\mathbf{x}} = (\,I_{n\times n} \quad -I_{n\times n}\,)\mathbf{X} = H_e\mathbf{X} \tag{71}$$

the covariance of the true navigation errors before the event trigger $P_{\text{true}} = H_e\mathcal{C}_A(\bar{t}_e)H^T_e$ is equal to the covariance of the true navigation error after the event trigger $P^+_{\text{true}} = H_e\Phi_S\mathcal{C}^+_A(t_e)\Phi^T_S H^T_e$. In other words, the shaping matrix Φ_s leaves the covariance of the true navigation error unchanged, as expected.

V. Event Triggers in Orbital Rendezvous Applications

We now return to the coelliptic approach phase of an orbital rendezvous, where a chaser vehicle approaches an object from behind and below with a near constant relative altitude and relative velocity. Instead of using time, a well-known orbital rendezvous technique is to trigger a terminal phase initiation maneuver when the apparent elevation of the object is equal to 28 deg. When the object is at the desired elevation angle (as indicated by navigation), the TPI maneuver is used to transfer the chaser to a position on the object v-bar.

To simulate this elevation trigger, we must specify the nominal state vector of the TPI maneuver at the nominal time of the elevation-angle trigger,

$$\bar{\mathbf{x}}(\bar{t}_e) = \begin{pmatrix}\bar{\mathbf{r}}^i_o(\bar{t}_e)\\ \bar{\mathbf{v}}^i_o(\bar{t}_e)\\ \bar{\mathbf{r}}^i_c(\bar{t}_e)\\ \bar{\mathbf{v}}^i_c(\bar{t}_e)\end{pmatrix} \tag{72}$$

the associated nominal time-derivatives of the states,

$$\dot{\bar{\mathbf{x}}}(\bar{t}_e) = \begin{pmatrix}\dot{\bar{\mathbf{r}}}^i_o(\bar{t}_e)\\ \dot{\bar{\mathbf{v}}}^i_o(\bar{t}_e)\\ \dot{\bar{\mathbf{r}}}^i_c(\bar{t}_e)\\ \dot{\bar{\mathbf{v}}}^i_c(\bar{t}_e)\end{pmatrix} = \begin{pmatrix}\bar{\mathbf{v}}^i_o(\bar{t}_e)\\ \mathbf{F}^i_{\text{grav}_o}[\bar{\mathbf{r}}^i_o(\bar{t}_e)]\\ \bar{\mathbf{v}}^i_c(\bar{t}_e)\\ \mathbf{F}^i_{\text{grav}_c}[\bar{\mathbf{r}}^i_c(\bar{t}_e)]\end{pmatrix} \tag{73}$$

and the trigger condition,

$$\Psi[\hat{\mathbf{x}}(t_e)] = \frac{[\mathbf{r}^i_o - \mathbf{r}^i_c]}{|\mathbf{r}^i_o - \mathbf{r}^i_c|}\cdot\mathbf{i}^i_{\mathbf{v}_o}(\mathbf{r}^i_o, \mathbf{v}^i_o) - \cos(28\ \text{deg}) \tag{74}$$

This equation is valid for near-circular orbits. A more complicated expression can be derived for orbits with arbitrary eccentricity.

If the augmented state covariance matrix at the nominal time of the trigger is $\mathcal{C}_A(\bar{t}_e)$, we can compute the effect of the elevation-angle trigger on the state covariance by using Eq. (69), repeated here for convenience:

$$\mathcal{C}_A^+(\bar{t}_e) = E[\mathbf{X}(t_e)\mathbf{X}^T(t_e)] = \Phi_S \mathcal{C}_A(\bar{t}_e)\Phi_S^T$$

where Φ_S is the shaping matrix in Eq. (70).

The covariance of the relative position dispersions in lvlh coordinates at the nominal trigger time $\bar{t}_e$ is given by

$$D_{\text{lvlh}}(\bar{t}_e) = H_{\text{lvlh}}\mathcal{C}_A(\bar{t}_e)H_{\text{lvlh}}^T \tag{75}$$

After the trigger, the covariance of the relative position dispersions in lvlh coordinates is given by

$$D_{\text{lvlh}}^+(\bar{t}_e) = H_{\text{lvlh}}\mathcal{C}_A^+(\bar{t}_e)H_{\text{lvlh}}^T \tag{76}$$

where, in both cases,

$$H_{\text{lvlh}} = (\,\mathcal{T}^i_{\text{lvlh}}(\bar{\mathbf{r}}^i_o, \bar{\mathbf{v}}^i_o) \quad 0_{3\times3} \quad -\mathcal{T}^i_{\text{lvlh}}(\bar{\mathbf{r}}^i_o, \bar{\mathbf{v}}^i_o) \quad 0_{3\times3} \quad 0_{3\times n}\,) \tag{77}$$

Figure 4 illustrates what we might expect for this type of orbital rendezvous problem. The figure shows a nominal trajectory with two Monte Carlo samples. In all cases, the TPI maneuvers occur at the desired elevation angle, independent of the variation in chaser orbital energy. This should be compared with the case without the elevation-angle trigger in Fig. 2.

Figure 4 also shows the anticipated covariance ellipses, but when we employ the new event trigger equations [Eqs. (69) and (70)] in the linear covariance analysis, the covariance ellipses are not as expected. In fact, the linear covariance results in Fig. 5 are not even close to the anticipated results. It turns out that the problem is not in the event trigger equations, but in the expression for H_{lvlh} in Eq. (77), which is used to determine the lvlh dispersion covariance.

Notice that, when target position and velocity dispersions are small, it is reasonable to use

$$\mathbf{R}^{\text{lvlh}} = \mathcal{T}^i_{\text{lvlh}}(\bar{\mathbf{r}}^i_o, \bar{\mathbf{v}}^i_o)[\mathbf{r}^i_o - \mathbf{r}^i_c] \tag{78}$$

to compute the relative position in lvlh coordinates for each Monte Carlo sample. The partial derivative of this expression with respect to the augmented states produces H_{lvlh} given in Eq. (77). However, if the dispersions of the target position and velocity are large, it becomes more accurate to use Eq. (79) to compute the relative position in lvlh coordinates for each Monte Carlo sample:

$$\mathbf{R}^{\text{lvlh}} = \mathcal{T}^i_{\text{lvlh}}(\mathbf{r}^i_o, \mathbf{v}^i_o)[\mathbf{r}^i_o - \mathbf{r}^i_c] \tag{79}$$

Taking the partial derivative of this equation with respect to the augmented states produces

$$H_{\text{lvlh}} = (\,\mathcal{T}^i_{\text{lvlh}}(\bar{\mathbf{r}}^i_o, \bar{\mathbf{v}}^i_o) \quad 0_{3\times3} \quad -\mathcal{T}^i_{\text{lvlh}}(\bar{\mathbf{r}}^i_o, \bar{\mathbf{v}}^i_o) \quad 0_{3\times3} \quad 0_{3\times n}\,) + \begin{pmatrix} 0_{1\times3} & [\bar{\mathbf{R}}^i]^T\{I_{3\times3} - [\mathbf{i}^i_{\mathbf{v}_o}][\mathbf{i}^i_{\mathbf{v}_o}]^T\}/|\bar{\mathbf{v}}_o| & 0_{1\times6} & 0_{1\times n} \\ \frac{-[\bar{\mathbf{R}}^i]^T\{I_{3\times3} - [\mathbf{i}^i_{\mathbf{h}_o}][\mathbf{i}^i_{\mathbf{h}_o}]^T\}[\bar{\mathbf{v}}^i_o\times]}{|\mathbf{h}_o|} & \frac{[\bar{\mathbf{R}}^i]^T\{I_{3\times3} - [\mathbf{i}^i_{\mathbf{h}_o}][\mathbf{i}^i_{\mathbf{h}_o}]^T\}[\bar{\mathbf{r}}^i_o\times]}{|\mathbf{h}_o|} & 0_{1\times6} & 0_{1\times n} \\ (\bar{\mathbf{R}}^i)^T\{I_{3\times3} - [\mathbf{i}^i_{\mathbf{r}_o}][\mathbf{i}^i_{\mathbf{r}_o}]^T\}/|\bar{\mathbf{r}}_o| & 0_{1\times3} & 0_{1\times6} & 0_{1\times n} \end{pmatrix} \tag{80}$$

If we use this expression for H_{lvlh} to compute and plot the relative position dispersion ellipses, we obtain the expected results shown in Fig. 6.

One question remains: Why does the simpler version of H_{lvlh} seem to work fine only until an event trigger is implemented? The answer lies in the level of the inertial dispersions of the target position and velocity. When the dispersions are small (e.g., <1 km in position), the associated dispersed lvlh frames are not very far from the nominal lvlh frame. However, when an elevation-angle trigger is implemented, the time of the TPI maneuver can vary by hundreds of seconds. Because the inertial velocity of the target is 7.5 km/s in low Earth orbit, the inertial position of the target at TPI can vary by thousands of kilometers. The effect is illustrated in Figs. 7 and 8.

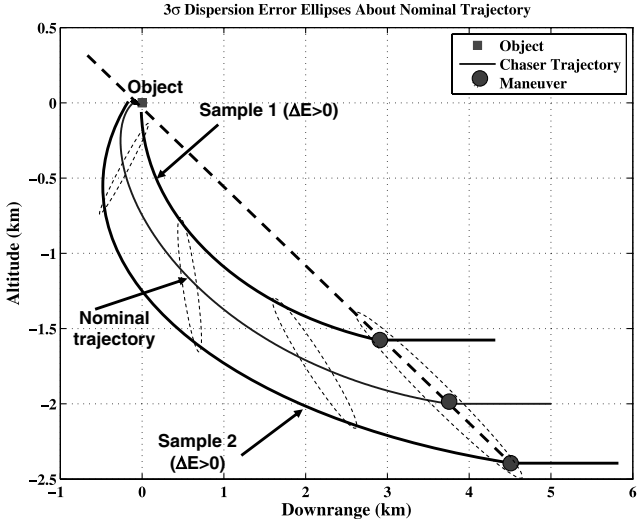

Fig. 4 Example of two Monte Carlo samples of a 2 km coelliptic approach. TPI occurs at a fixed elevation angle and initiates a 130 deg orbital (inertial) transfer. Navigation errors are <3 m 3-σ, and Δv execution errors are <3 mm/s 3-σ. Although the orbital energy of samples 1 and 2 are different than the nominal, TPI always occurs at the desired elevation angle. Anticipated dispersion covariance ellipses are also shown.

VI. Quantitative Analysis of Elevation-Angle Triggers

In this section, we study the effect and advantage of using elevation-angle triggers for orbital rendezvous. In the analysis that follows, it is assumed that a chaser vehicle is approaching a target vehicle from behind and below on a coelliptic approach. The chaser is initially 10 km behind and 1 km below the target in a low Earth orbit. The initial trajectory dispersions and navigation errors are shown in Table 1. For navigation, a Lidar system onboard the chaser is used to determine the relative position of the target. Relative navigation accuracies are also shown in Table 1. When the target is at the desired elevation angle during the coelliptic approach (as determined by the chaser onboard navigation system), a transfer phase initiation maneuver is executed to transfer the chaser from the coelliptic approach to a trajectory that intercepts the target in a specified amount of time.

To illustrate the advantages of using an elevation-angle trigger instead of a time trigger for the TPI maneuver, a linear covariance analysis program based on the models in Secs. III and V was used to determine the required TPI maneuver Δv to intercept the target for a fixed 130 deg orbital transfer from TPI to intercept. The results shown in Fig. 9 are a function of the desired elevation angle at TPI. The top plot shows the nominal TPI Δv, and the bottom plot shows the sum of the nominal and 3-σ variation in the TPI Δv. For trigger angles in the range of 20–30 deg, there is clearly a significant savings in terms of the required 3-σ TPI Δv.

Additionally, there are significant improvements in trajectory dispersions when elevation-angle triggers are used. Figure 10 shows the in-plane and out-of-plane 3-σ relative position dispersions for

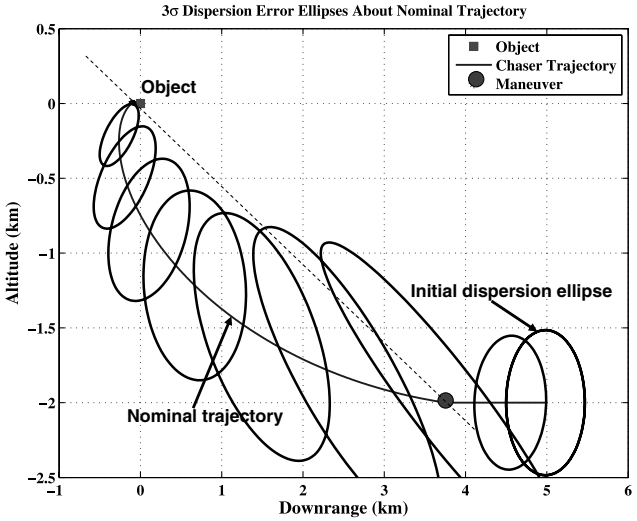

Fig. 5 Incorrect linear covariance analysis results for a 2 km coelliptic approach. TPI occurs at a fixed elevation angle and initiates a 130 deg orbital (inertial) transfer.

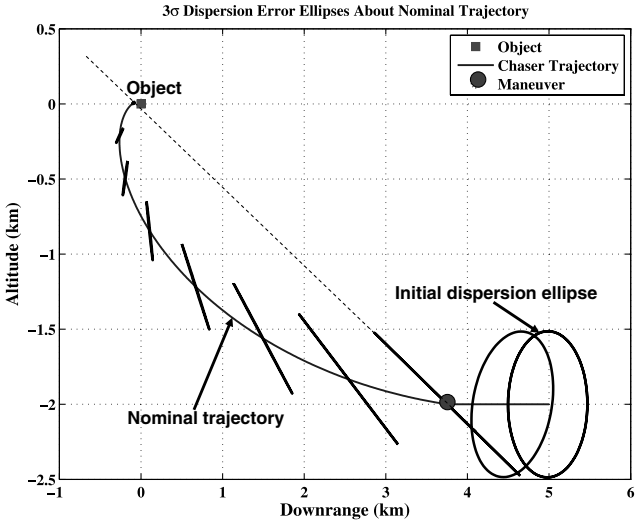

Fig. 6 Correct linear covariance analysis results for a 2 km coelliptic approach. TPI occurs at a fixed elevation angle and initiates a 130 deg orbital (inertial) transfer.

time-triggered maneuvers (top plots) and elevation-angle triggered maneuvers (bottom plots). For both cases, three different elevation angles at TPI were examined. Notice that the elevation-angle trigger significantly improved the in-plane 3-σ dispersions. Because the elevation-angle trigger is based only on in-plane conditions, it had no effect on the out-of-plane dispersions. Notice also that, although the 37.5 deg elevation-angle trigger produced the lowest dispersions, the 27.5 deg trigger produced the best combination of low dispersions and 3-σ Δv (see Figs. 9 and 10). Figure 11 shows the relative in-plane position dispersion ellipses when a TPI maneuver is triggered on time and nominally executed at an elevation angle of 27.5 deg, and

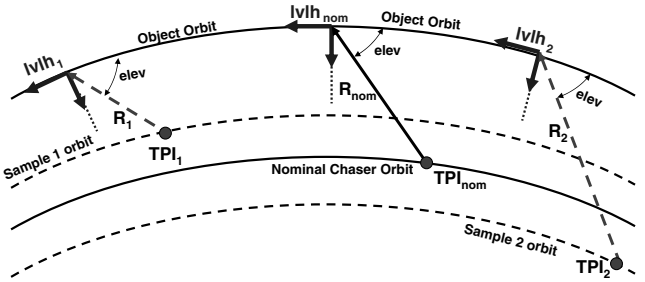

Fig. 7 Inertial perspective of the nominal trajectory and two Monte Carlo samples. TPI is triggered by elevation angle. Sample 1 has a slightly higher orbital energy than nominal and therefore initiates the transfer later in time. The opposite is true for sample 2.

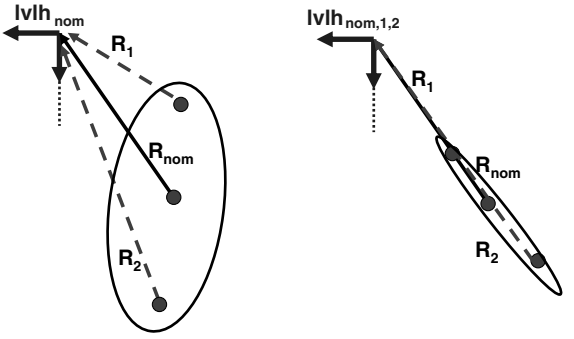

Fig. 8 On the left, the relative position vectors from Fig. 7 (R_1, R_{nom}, and R_2) are plotted in the nominal lvlh frame. On the right, the same vectors are plotted in their respective lvlh frames. Results on the right are clearly what is desired.

Fig. 12 shows the resulting in-plane relative position dispersion ellipses when a TPI maneuver is triggered on elevation angle and nominally executed at the same elevation angle. The differences are remarkable. The elevation-angle trigger clearly shows better trajectory dispersion control.

The preceding analysis was limited to an arbitrarily selected 130 deg orbital transfer from TPI to intercept. A natural extension to this analysis is to consider additional orbital transfer angles. Figure 13 shows the Δv results for a variety of orbital transfer angles when TPI is triggered by an elevation angle. The top plot shows that the nominal Δv decreases monotonically with orbital transfer angle for each trigger elevation angle. The 170 deg orbital transfer shows the lowest Δv. This is to be expected, as the absolute minimum nominal Δv can be achieved with a 180 deg orbital transfer.

The 3-σ TPI Δv results shown in the bottom plot of Fig. 13, however, show some very interesting and unexpected properties. The 170 deg orbital transfer no longer yields the lowest Δv. In fact, the 170 deg case is now one of the worst cases, as is the fastest 90 deg transfer. In terms of 3-σ TPI Δv, the best cases have an orbital transfer angle between 130–150 deg and an elevation-angle trigger between 20–28 deg, ranges used for the Apollo and Gemini missions [1,2,4].

The effect of orbital transfer angle on trajectory dispersions is shown in Fig. 14. At large range (>500 m), the in-plane dispersions are relatively insensitive to the orbital transfer angle and are smaller

Table 1 Initial target and chaser position/velocity dispersions, navigation errors, and Lidar instrument errors

Error source	Value
Initial position/velocity dispersions, 3-σ	500 m downrange, 0.1 m/s downrange rate
	100 m cross track, 0.1 m/s cross-track rate
	100 m altitude, 0.5 m/s altitude rate
	−0.9 correlation in the downrange/altitude rate, altitude/downrange rate channels
Relative navigation errors, 3-σ	Position error, <3 m/axis
	Velocity error, <3 mm/s per axis

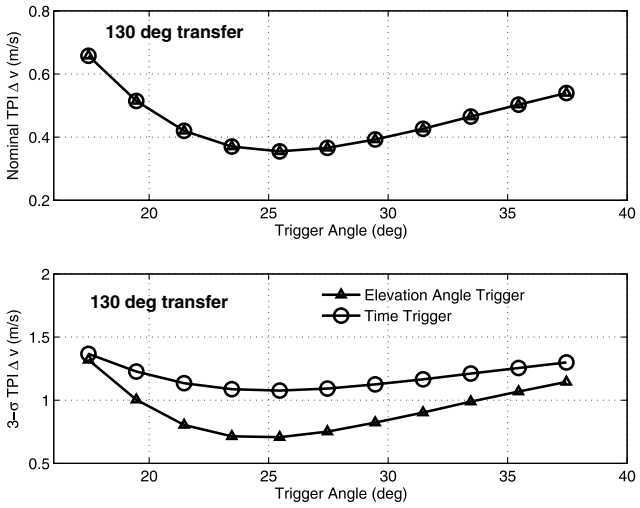

Fig. 9 Nominal TPI Δv (top) as a function of elevation angle at TPI for a 130 deg orbital transfer. Nominal plus 3-σ (bottom) variation in the TPI Δv for both time-triggered maneuvers and elevation-angle maneuvers as a function of elevation angle at TPI.

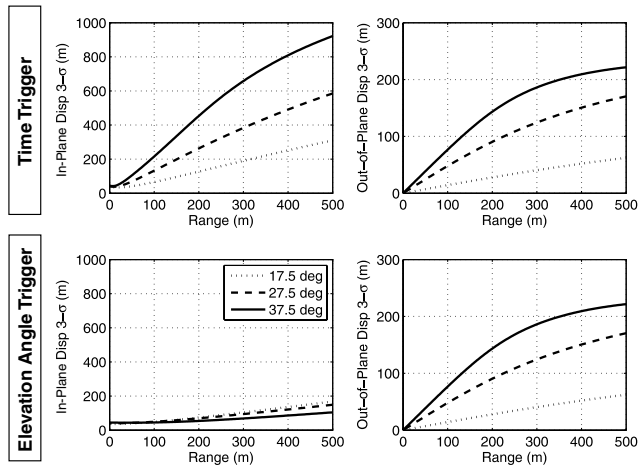

Fig. 10 In-plane and out-of-plane position dispersions as a function of range from the target for three different elevation angles at TPI. In the top plots, TPI is triggered on time. In the bottom plots, TPI is triggered in elevation angle. The orbital transfer angle from TPI to intercept is 130 deg. Navigation errors are <3 m 3-σ, and Δv execution errors are <3 mm/s 3-σ.

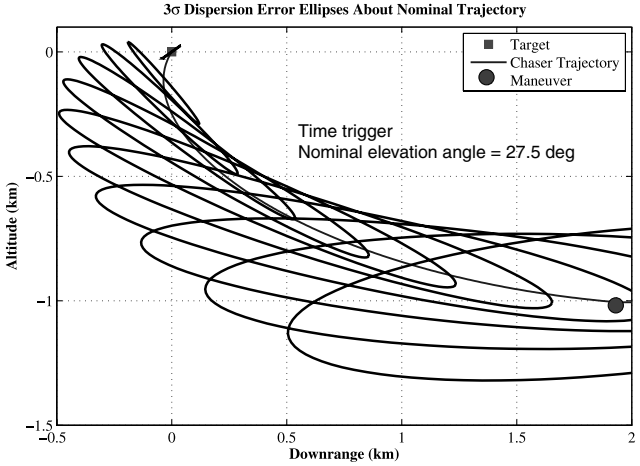

Fig. 11 In-plane relative position dispersion ellipses when a TPI maneuver is triggered on time and nominally executed at an elevation angle of 27.5 deg. The orbital transfer angle from TPI to intercept is 130 deg.

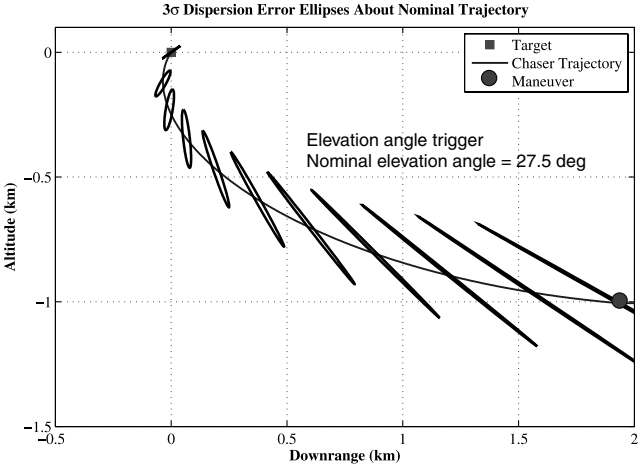

Fig. 12 In-plane relative position dispersion ellipses when a TPI maneuver is triggered on elevation angle and nominally executed at an elevation angle of 27.5 deg. The orbital transfer angle from TPI to intercept is 130 deg.

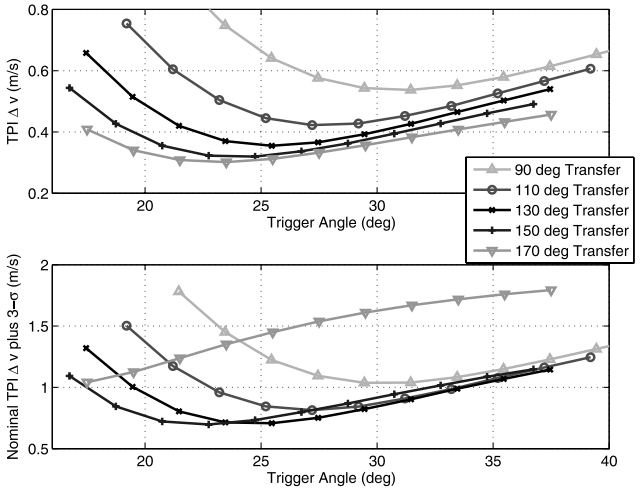

Fig. 13 Nominal TPI Δv (top) as a function of elevation angle at TPI for several orbital transfer angles. 3-σ variation (bottom) in the TPI Δv as a function of elevation angle at TPI.

with increasing trigger elevation angle. At small distances (<50 m), the in-plane dispersions are insensitive to the trigger elevation angle and are smaller with faster transfer times. In terms of in-plane position dispersions, the elevation-angle trigger produces a large improvement over a time trigger (see Fig. 10), but only relatively small additional improvements can be made by varying the orbital transfer angle or the elevation angle of the trigger.

On the other hand, in terms of out-of-plane position dispersions, an elevation-angle maneuver trigger produces no improvement over a time-based maneuver trigger (again, see Fig. 10). However, out-of-plane dispersions are sensitive to the choice of TPI elevation angle and very sensitive to the choice orbital transfer angle. The fact that large orbital transfer angles produce large out-of-plane position dispersions is directly related to a problem encountered in Lambert targeting when the transfer angle is near 180 deg.

In reviewing Figs. 13 and 14, it is clear the 170 deg transfer case produces position dispersions that are too large to be considered, and the 90 deg transfer case requires to much 3-σ Δv to be considered. Thus, in Fig. 15, we see the total 3-σ position dispersions for the three remaining orbital transfer angles that were considered (110, 130, and 150 deg) as a function of range and the three elevation-angle triggers. It can be seen that the 110 deg transfer cases are relatively insensitive to trigger elevation angle. The best 110 deg transfer case is achieved with an elevation angle of approximately 27.2 deg which

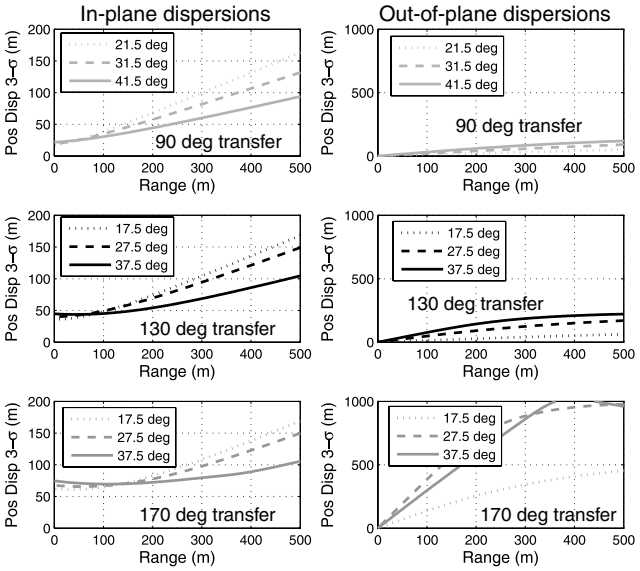

Fig. 14 In-plane and out-of-plane position dispersions as a function of range from the target for three different elevation angles at TPI and three different orbital transfer angles.

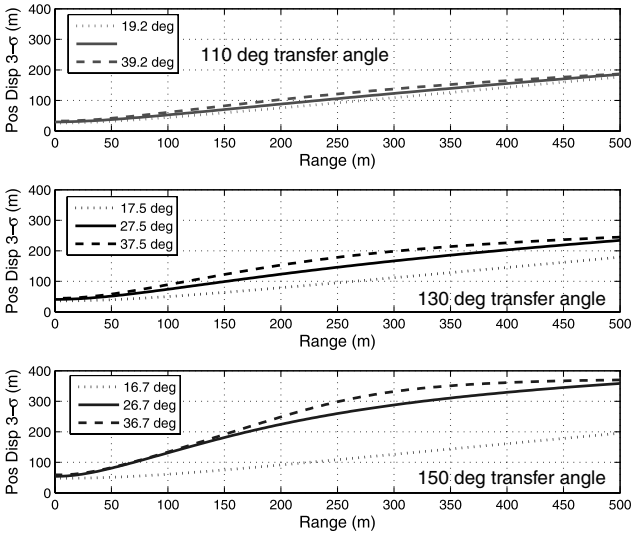

Fig. 15 Total 3-σ position dispersions for the three orbital transfer angles and three trigger elevation angles as a function of range and the three elevation-angle triggers.

corresponds to a maximum 3-σ position dispersion of 185 m and a 3-σ Δv of 0.7 m/s (see Fig. 13). The 150 deg transfer has very low 3-σ Δv characteristics near elevation angles of 20–25 deg, but the corresponding maximum position dispersions are approximately 300 m 3-σ. The 130 deg transfer case appears to have to the best combination of 3-σ Δv characteristics and 3-σ dispersion characteristics. With an orbital transfer angle of 130 deg and an elevation angle of 25.5 deg, a maximum 3-σ position dispersion of approximately 200 m and a 3-σ Δv of only 0.5 m/s can be achieved.

VII. Conclusions

We have developed and documented new equations to implement a generic event trigger in a linear covariance analysis. Over time, these equations will find their way into many linear covariance simulations and many different applications.

We have shown that these equations have an immediate application in GN&C orbital rendezvous when an elevation angle is used to trigger a TPI maneuver. Our analysis has shown that the event trigger equations are accurate and can be used for orbital rendezvous elevation-angle triggers. However, we have found that it is very important to recognize that TPI maneuver-time variations can induce large inertial dispersions in the target states. These dispersions can produce large variations in the orientation of the target-centered lvlh frame from the nominal and need to be taken into account when conducting linear covariance analysis for orbital rendezvous problems.

It has been clearly demonstrated that an elevation-angle trigger in orbital rendezvous is useful in reducing trajectory dispersions and maneuver Δv. It has also been demonstrated that a trigger angle in the range of 25–28 deg, in combination with an orbital transfer angle in the range of 110–130 deg, will provide the best balance of maneuver Δv and relative position dispersions for target intercept trajectories in low Earth orbit.

Appendix: Matrix Partial Derivatives and Process Noise

The covariance of the state process noise given by

$$\hat{S}_w = \begin{pmatrix} \hat{S}_{w_o} & 0_{6\times6} \\ 0_{6\times6} & \hat{S}_{w_c} \end{pmatrix} \tag{A1}$$

and the partial derivatives of the state dynamics with respect to the states are

$$\hat{F}_{\hat{x}} = \begin{pmatrix} \hat{F}_{\hat{x}_o} & 0_{6\times6} \\ 0_{6\times6} & \hat{F}_{\hat{x}_c} \end{pmatrix} \tag{A2}$$

where

$$\hat{S}_{w_o} = \begin{pmatrix} 0_{3\times3} & 0_{3\times3} \\ 0_{3\times3} & \hat{S}_{g_o} \end{pmatrix} \tag{A3}$$

$$\hat{S}_{w_c} = \begin{pmatrix} 0_{3\times3} & 0_{3\times3} \\ 0_{3\times3} & \hat{S}_{g_c} \end{pmatrix} \tag{A4}$$

and

$$\hat{F}_{\hat{x}_o} = \begin{pmatrix} 0_{3\times3} & I_{3\times3} \\ \hat{m}_o^{-1}\partial\mathbf{F}^i_{\text{grav}_o}/\partial\hat{\mathbf{r}}^i_o & 0_{3\times3} \end{pmatrix} \tag{A5}$$

$$\hat{F}_{\hat{x}_c} = \begin{pmatrix} 0_{3\times3} & I_{3\times3} \\ \hat{m}_c^{-1}\partial\mathbf{F}^i_{\text{grav}_c}/\partial\hat{\mathbf{r}}^i_c & 0_{3\times3} \end{pmatrix} \tag{A6}$$

The state and state covariance correction matrix is given by

$$\hat{D}_{\hat{x}} = \begin{pmatrix} 0_{3\times3} & 0_{3\times3} & 0_{3\times3} & 0_{3\times3} \\ \frac{\partial\Delta v^i_{\text{com}}}{\partial\hat{\mathbf{r}}^i_o} & \frac{\partial\Delta v^i_{\text{com}}}{\partial\hat{\mathbf{v}}^i_o} & \frac{\partial\Delta v^i_{\text{com}}}{\partial\hat{\mathbf{r}}^i_c} & \frac{\partial\Delta v^i_{\text{com}}}{\partial\hat{\mathbf{v}}^i_c} \\ 0_{3\times3} & 0_{3\times3} & 0_{3\times3} & 0_{3\times3} \\ 0_{3\times3} & 0_{3\times3} & 0_{3\times3} & 0_{3\times3} \end{pmatrix} \tag{A7}$$

References

[1] Burton, J., and Hayes, W., "Gemini Rendezvous," *Journal of Spacecraft and Rockets*, Vol. 3, No. 1, 1966, pp. 145–147. doi:10.2514/3.59526

[2] Miller, J. E., and Laats, A., "Apollo Guidance and Control System Flight Experience," *Journal of Spacecraft and Rockets*, Vol. 7, No. 5, May 1970, pp. 551–557. doi:10.2514/3.29989

[3] Pearson, D. J., "Shuttle Rendezvous and Proximity Operations," *Proceedings of the CNES International Symposium on Space Dynamics*, Centre National d' Etudes Spatiales, Cepadues Editions, Toulouse, France, 1989, pp. 833–851.

[4] Young, K. A., and Alexander, J. D., "Apollo Lunar Rendezvous," *Journal of Spacecraft and Rockets*, Vol. 7, No. 9, Sept. 1970, pp. 1083–1086. doi:10.2514/3.30106

[5] Geller, D. K., "Analysis of the Relative Attitude and Control Problem for Satellite Inspection and Orbital Rendezvous," *Journal of the Astronautical Sciences*, Vol. 55, No. 2, 2007, pp. 195–214.
[6] Geller, D. K., "Linear Covariance Techniques for Orbital Rendezvous Analysis and Autonomous On-Board Mission Planning," *Journal of Guidance, Control, and Dynamics*, Vol. 29, No. 6, 2006, pp. 1404–1414.
doi:10.2514/1.19447
[7] Geller, D. K., "Orbital Rendezvous: When is Autonomy Required?" *Journal of Guidance, Control, and Dynamics*, Vol. 30, No. 4, 2007, pp. 974–981.
doi:10.2514/1.27052
[8] Woffinden, D., and Geller, D., "Relative Angles-Only Navigation and Pose Estimation for Autonomous Orbital Rendezvous," *Journal of Guidance, Control, and Dynamics*, Vol. 30, No. 5, 2007, pp. 1455–1469.
doi:10.2514/1.28216
[9] Gelb, A. (ed.), "Applied Optimal Control," MIT Press, Cambridge, MA, 1974.
[10] Maybeck, P. S., *Stochastic Models, Estimation, and Control*, Academic Press, New York, 1979.
[11] Vallado, D. A., *Fundamentals of Astrodynamics and Applications*, McGraw–Hill, New York, 1997, pp. 343–366.